LETTER • OPEN ACCESS

Possible influence of the warm pool ITCZ on compound climate extremes during the boreal summer

ENVIRONMENTAL RESEARCH
LETTERS

LETTER

Possible influence of the warm pool ITCZ on compound climate extremes during the boreal summer

Joseph Basconcillo[1,2], **Il-Ju Moon**[1,*], **Bin Wang**[3] **and Malcolm Mistry**[4,5]

[1] Typhoon Research Center, Jeju National University, Jeju, Republic of Korea
[2] Philippine Atmospheric, Geophysical and Astronomical Services Administration, Department of Science and Technology, Quezon City, Philippines
[3] School of Ocean and Earth Science and Technology, University of Hawaii, Honolulu, HI, United States of America
[4] Department of Public Health, Environments and Society, London School of Hygiene & Tropical Medicine (LSHTM), London, United Kingdom
[5] Department of Economics, Ca' Foscari University of Venice, Venice, Italy
[*] Author to whom any correspondence should be addressed.

E-mail: ijmoon@jejunu.ac.kr

Keywords: compound climate extremes, tropics, Arctic, tropical cyclones, warm pool ITCZ

Supplementary material for this article is available online

OPEN ACCESS

RECEIVED
24 August 2021

REVISED
7 October 2021

ACCEPTED FOR PUBLICATION
19 October 2021

PUBLISHED
2 November 2021

Abstract

In a globally changing climate, there is a growing concern for understanding and predicting compound climate extremes. However, the relationship of compound climate extremes with each other has been mostly analyzed in isolation and/or on regional scales. Little attention has been paid to their simultaneous occurrence and compound impacts worldwide. Here we demonstrate that the compound climate extremes in the Northern Hemisphere during the boreal summer are interconnected from the tropics to the Arctic. This connection originates from the interannual variations of the Indo-Pacific warm pool's intertropical convergence zone (ITCZ). We demonstrate that the warm pool ITCZ (WPI) convection possibly influences three major teleconnection patterns (i.e. zonal, meridional, and circumglobal) where compound climate extremes occur along the wave train excited by the WPI convection. Most notably, the WPI can sufficiently explain climate variabilities in the North Atlantic region, which influences the occurrence of compound climate extremes in many parts of Europe and North America. Our findings advance the understanding of the interannual global/regional variability of climate extremes and are potentially valuable for predicting seasonal high-impact climate extremes.

1. Introduction

Our planet is warming—up fast. The Intergovernmental Panel on Climate Change (IPCC) reported that one reason for concern under global warming is the increased risk for climate extremes like heatwaves, heavy rain, drought, wildfires, and flooding (Intergovernmental Panel on Climate Change (IPCC) 2021). Consequentially, it has become a growing motivation for the scientific community to understand the variability of compound climate extremes for effective disaster risk reduction and preparedness.

Notably, the 2018 boreal summer (June–July–August; JJA) was marked by the widespread occurrence of compound climate extremes (figure 1). For example, the tropics experienced extreme rainfall, flooding, and landslides, and highlighted by the highest tropical cyclone (TC) frequency in the Western North Pacific (WNP) (figure 2(a)) (Wang *et al* 2019, Basconcillo *et al* 2021) that has simultaneously occurred with the highest WNP summer monsoon index (WNPMI) since 1984 (Basconcillo *et al* 2021). Meanwhile, wildfires, prolonged dry conditions, and heatwaves were also reported in many parts of the Northern Hemisphere (NH) midlatitudes including the United States and Alaska, Canada, East Asia, Eurasia, and Europe (supplementary table S1 (available online at stacks.iop.org/ERL/16/114039/mmedia)).

One theory that explains the occurrence of compound climate extremes, particularly in the NH midlatitudes, is through the influence of the Arctic

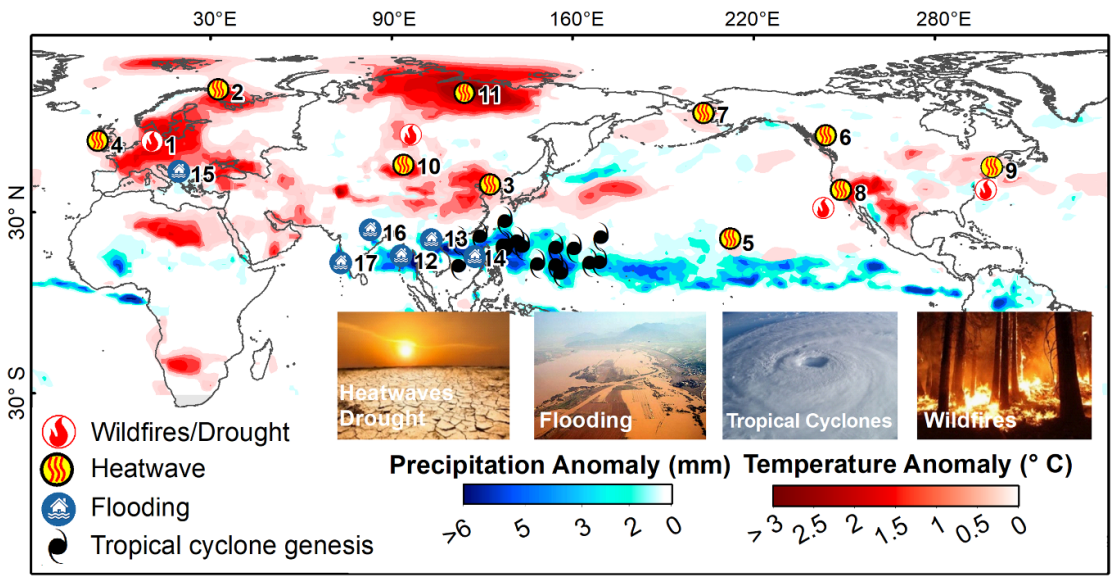

Figure 1. Co-occurrence of compound climate extremes during the 2018 boreal summer. The blue (red) shades indicate positive precipitation (temperature) anomalies. Each climate extreme is indexed as wildfires/drought, heatwave or consecutive warm days, heavy precipitation/flooding, and tropical cyclone genesis, respectively. For example, the 2018 heatwave in East Asia is shown here as Point No. 3 with icon corresponding to heatwave. The details of these events and their impacts are provided in supplementary table S1. (Inset images credit: Wildfire—Mike McMillan, US Forest Service; Tropical Cyclones—NASA Johnson Space Center; Heatwave—Tom Yang, Shutterstock).

climate on the subtropical jetstream (Francis and Vavrus 2012, Cohen *et al* 2014, Coumou *et al* 2018). It is widely thought that an anomalous Arctic warming results in a weakened and wavier subtropical jetstream, which allows warm (cold) air mass from the tropics (Arctic) to stall and lead to the occurrence of heatwaves (cold waves) in many parts of midlatitudes. Considering that the Arctic summer is less variable than the Arctic winter (Bintanja and van der Linden 2013), it is more likely that the different regional/local modes of Arctic variabilities have more active regional influence during the boreal summer. For example, the North Atlantic oscillation (NAO) uses the mean sea-level pressure difference over the Icelandic and Azores regions, and the Greenland blocking index (GBI) applies the mean 500 hPa geopotential height in the Greenland region to explain the undulation of the North Atlantic subtropical jetstream and regional precipitation patterns in many parts of Europe and North America (Hanna *et al* 2013, Trouet *et al* 2018). However, such proposed pathway does not clearly represent a picture of how the warm tropical air mass or cold Arctic air mass is transported beyond the NH midlatitudes. Therefore, this explanation becomes insufficient in describing how the Arctic variabilities extend its influence on the tropics.

Another pathway that explains the development of compound climate extremes in the NH midlatitudes is through the meridional influence of tropical convective activities (Nitta 1987, Wang and Fan 1999, Wang *et al* 2001, Wakabayashi and Kawamura 2004, Watt-Meyer and Frierson 2018, Song *et al* 2018a, 2018b). As the risen moist air mass from the tropical convective heat sources meridionally moves poleward it loses moisture and becomes warm and dry as it descends vertically, which exacerbates dry conditions in the NH midlatitudes (Staten *et al* 2018). In this perspective, the tropical convective heat sources excite poleward momentum and energy exchange that triggers climate variabilities in the meridional direction. During the boreal summer, the NH tropics receive more solar insolation, thus, have energy surplus than the poleward branches of the meridional circulation (i.e. poleward Hadley Cell, Ferrel Cell, Polar Cell). Such net energy imbalance drives large-scale meridional heat engine to sustain poleward excess energy redistribution. Hence, of the said two pathways, the tropical convective heat sources can jumpstart the meridional circulation in driving poleward momentum and heat exchange that affect global climate anomaly patterns.

We recognize that there are already a number of existing tropical convection and teleconnection indices, and we do not attempt to discount their merits. Instead, we aim to present observational evidence that some of these indices could not totally capture notable midlatitude climate modes such as the NAO and the GBI, which are important in describing interannual climate variations in North America and Europe. Here we propose a tropical convection index called the warm pool ITCZ (WPI) index characterized by the interannual variations in

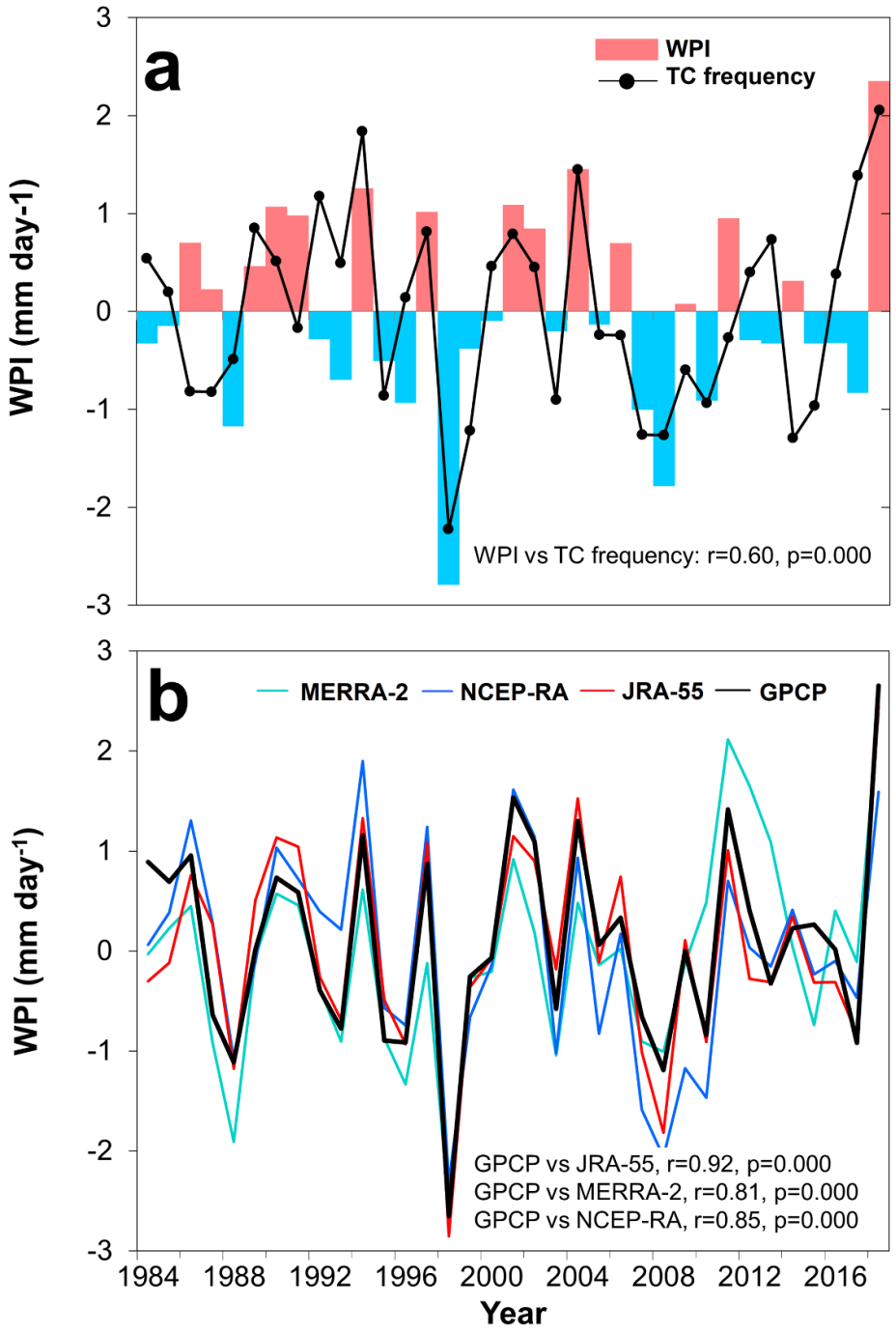

Figure 2. Timeseries of the WPI. (a) Timeseries of the WPI (bar), and TC frequency (black), respectively. (b) Timeseries of the WPI from the gridded precipitation values of GPCP (black) is used to compare with JRA-55 (red), MERRA-2 (cyan), and NCEP-RA (blue). JRA-55 is shown to have the highest correlation with GPCP, followed by MERRA-2, and NCEP-RA, respectively. In (a), the WPI is shown using JRA-55. In (a) and (b), the inset coefficients indicate the correlation of the indicated timeseries with each other.

the Indo-Pacific warm pool precipitation that possibly influence changes in the poleward branches of meridional circulation, and consequentially initiates a waveguide for the circumglobal teleconnection (Ding and Wang 2005, Ding *et al* 2011) of compound extreme events. Among these climate extremes include the active TC activity in the WNP, heavy precipitation in many parts of the tropics, and prolonged dry conditions in the NH midlatitudes.

2. Materials and methods

2.1. Reanalysis and TC best track dataset

Parallel to the reported reliable period of WNP TC observation data that extends back to the mid-1980s (Kang and Elsner 2012, Kim and Moon 2021), the timeseries analyses in our study (unless otherwise stated) were made uniform from 1984 to 2018. The TC best track data were obtained from the

International Best Track Archive for Climate Stewardship version 4 (Knapp *et al* 2010). Only named TCs in the WNP during JJA with maximum sustained winds of at least 35 knots (~17 ms^{-1}) were selected in our analysis.

When compared with the quasi-observed gridded precipitation from the Global Precipitation Climatology Project version 2.3 (GPCP) (Adler *et al* 2003), the Japanese Reanalysis 55 year Project (Kobayashi *et al* 2015) (JRA-55, $r = 0.92$, $p = 0.000$) has the highest correlation with GPCP v2.3 followed by Modern Era Retrospective-Analysis for Research and Applications (MERRA-2) reanalysis (Rienecker *et al* 2011) and National Centers for Environmental Protection (NCEP) reanalysis (Kalnay *et al* 1996) (figure 2(b)), respectively. For this reason, we selected the JRA-55 as our choice of reanalysis data. The Takaya and Nakamura-based (Takaya and Nakamura 2001) wave activity flux is also one of the elements available in JRA-55. In analyzing the teleconnection patterns associated with the WPI, we used the 700 hPa level in the partial correlation map and composite map analyses to highlight non-orographic features (Gadgil 2018) without totally deviating away from the lower troposphere.

2.2. Meridional circulation and climate indices

The meridional circulation indices used in this study include the Hadley Cell index (Chen *et al* 2014), East Asian Subtropical Jetstream index (Huang *et al* 2014), WNP Subtropical High index (Wang *et al* 2013), and Ferrel Cell index (Li *et al* 2014) (see supplementary table S2 for the detailed description of each index). The climate indices that we used include the Niño 4 (NOAA 2020), Indian Ocean basin wide (IOBW) sea surface temperature (SST) (TCC 2020a), NAO (National Oceanic and Atmospheric Administration (NOAA) 2020), and GBI (National Oceanic and Atmospheric Administration (NOAA) 2020, Hanna *et al* 2013). The tropical convection and teleconnection indices that we analyzed are the WNPMI (Wang and Fan 1999, Wang *et al* 2001), East Asian summer monsoon index (EASMI) (Wang *et al* 2008, Song and Zhou 2014a, 2014b), Pacific-Japan (PJ) pattern (Wakabayashi and Kawamura 2004), Pacific North American (PNA) pattern (National Oceanic and Atmospheric Administration (NOAA) 2020), Circumglobal teleconnection index (CGTI) (Ding and Wang 2005, Ding *et al* 2011), Silk Road pattern (SRP) (Song *et al* 2013), and Pacific Walker circulation index (Vecchi *et al* 2006). Lastly, the long-term climate indices that we used include the Pacific decadal oscillation (PDO) (National Oceanic and Atmospheric Administration (NOAA) 2020), Interdecadal Pacific oscillation (IPO) (National Oceanic and Atmospheric Administration (NOAA) 2020), and Atlantic meridional oscillation (AMO) (National Oceanic and Atmospheric Administration (NOAA) 2020).

2.3. Climate extreme indices

The gridded climate extreme indices (1984–2018) used in this study come from an updated dataset described in (Mistry 2019). We selected three climate extreme indices in our analysis. The PRCPTOT or the total precipitation during wet days indicates heavy and extreme precipitation. The TX90P or the percentage of days when daily maximum temperature exceeds the 90th percentile denotes extreme temperatures. Lastly, the consecutive dry day (CDD) or the number of consecutive days shows the prolonged dry conditions. These three climate extreme indices describe the locations of the extreme wet and dry compound climate extremes shown in figure 1 and in supplementary table S1.

2.4. Statistical tests

All timeseries were standardized and detrended before performing statistical tests. The Pearson's correlation is used to measure bivariate and partial correlations. The significance of correlation and regression coefficients is tested using t-statistic with two-tailed distribution. The significance of trend in the timeseries used the nonparametric Mann–Kendall test, which measures the monotonic or consistently upward or downward trend of a timeseries (Mann 1945, Kendall 1975). Meanwhile, the periodicity of WPI from 1984–2018 used the Paul wavelet transform, which decomposes a timeseries using localized oscillatory function or wavelet to determine the modes of variability in time-frequency space while providing better representation of peak periods towards higher frequencies than the other wavelet methods (Torrence and Compo 1998). We reduced the influence of PDO from an indicated timeseries by detrending it with respect to PDO or by removing its difference from its least-square regression with PDO. Lastly, when indicated, we used the 1-2-1 technique in timeseries filtering (Emanuel 2005).

3. Results

3.1. The warm pool ITCZ (WPI) index

The variations in the meridional circulation in the NH can be estimated by various metrics such as the position and strength of the ITCZ, Hadley cell, and subtropical jetstream. Among these metrics, the Indo-Pacific WPI index, which represents one of the most dominant tropical convective activities during the boreal summer (Schneider *et al* 2014), is proposed as another form of the tropical convection index.

The WPI can be measured in two ways: using the mean precipitation (figure 2(a)) and the mean pressure vertical velocity (ω) anomalies (Schneider *et al* 2010) from 850 to 200 hPa at 4 °N–22 °N, 80 °E–180 °E. We used the WPI based on precipitation in our succeeding analyses because precipitation

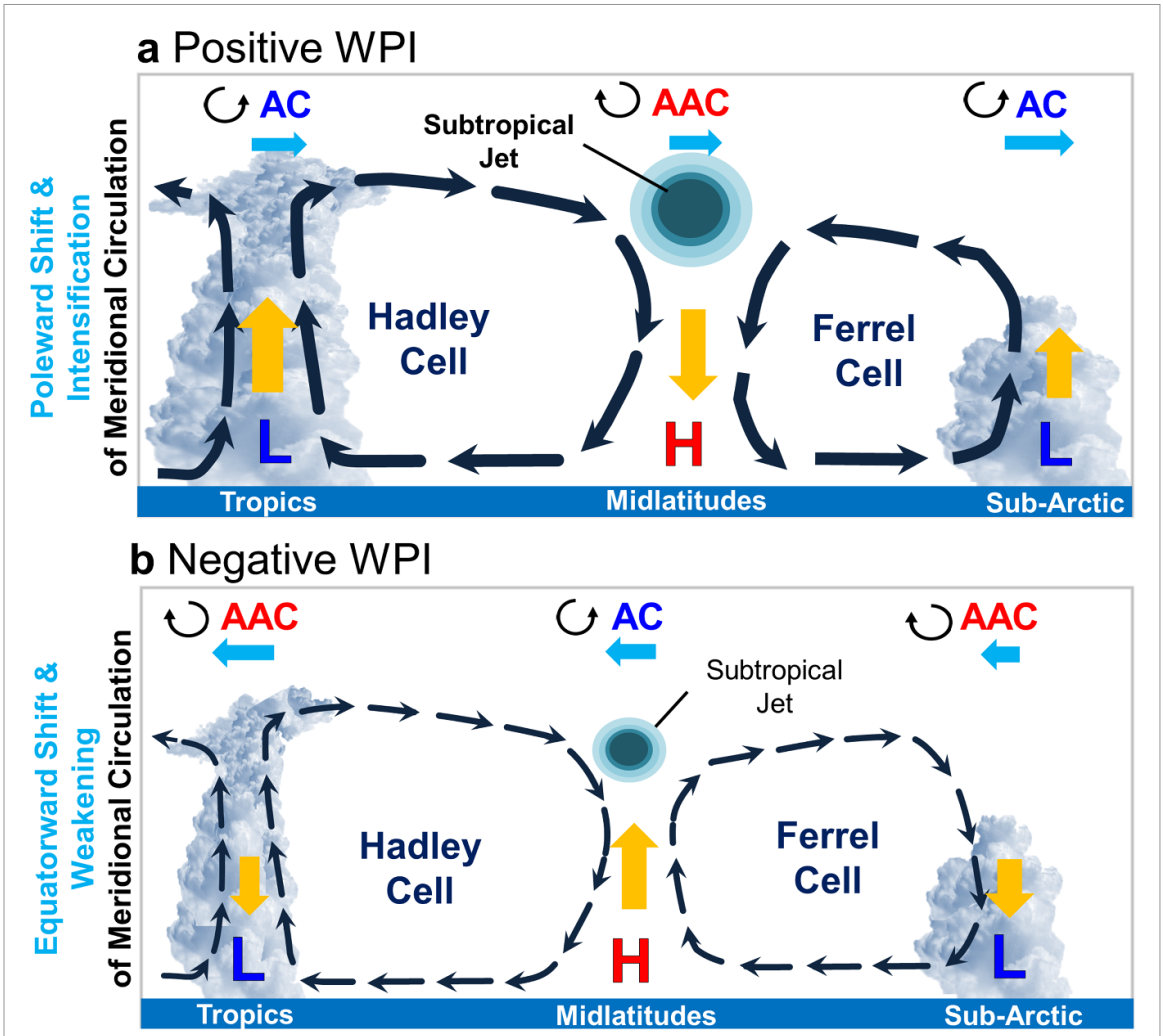

Figure 3. Schematic of the anomalous regional meridional circulation associated with the WPI. The WPI in its positive (a) and negative (b) phase during the boreal summer. The L (H) denotes a low (high) pressure region. AC (AAC) represents anomalous cyclonic circulation (anomalous anticyclonic circulation). The light blue (yellow) arrows represent direction of meridional shifts (anomalous ascent or descent of air mass). The convection in the WPI expands (contracts) with its boundaries shifting poleward (equatorward), which results to stronger (weaker) descent of dry air in the midlatitudes. The stronger (weaker) Hadley Cell and subtropical jetstream also shift poleward (equatorward) and prompt intensification (weakening) of the Ferrel Cell where it converges to an expanded (contracted) convection in the subpolar low.

is directly observable parameter unlike pressure vertical velocity. The domain of the WPI is the region with the strongest precipitation in the first leading empirical orthogonal function mode of precipitation during JJA from 1984–2018 (supplementary figures S1(a) and (b)). In the composite analysis, a positive (negative) WPI is defined as greater (less) than or equal to 0.9 standard deviation of the WPI timeseries from 1984 to 2018. The positive WPI years include 1990, 1991, 1994, 1997, 2001, 2004, 2011, and 2018. The negative WPI years are 1988, 1996, 1998, 2007, 2008, and 2010.

When the WPI is in its positive phase, the ITCZ intensifies, which is characterized by stronger convection in the WPI region (supplementary figures 2(a) and (d)) with its boundaries shifting poleward accompanied by strong descending warm and dry vertical flow in the midlatitudes (figures 3(a), 4(a) and (c)). Such relationship is corroborated by the significant correlation of the WPI with the following meridional circulation indices: WNP Subtropical High index ($r = -0.70$, $p = 0.000$), Hadley Cell index ($r = 0.69$, $p = 0.000$), Ferrel Cell index ($r = -0.64$, $p = 0.000$), and East Asian Subtropical Jetstream index ($r = 0.60$, $p = 0.000$) (table 1). A positive (negative) Hadley (Ferrel) Cell index indicates wider and stronger meridional circulation (figures 4(a) and (b)), poleward and stronger East subtropical jetstream (figures 4(d) and (e)), and northward-shifted WNP subtropical high (figure 5(d)). Meanwhile, the stronger convection and anomalous cyclonic vorticity in the WPI region provides favorable conditions for storm genesis and heavy precipitation in most parts of the tropics (figures 5(b), (h), (j)) (Evans 1993).

The SST in the central Pacific becomes warmer in a positive WPI phase (around 160 °E) (figure 5(f)), which is corroborated by the significant correlation of WPI with Niño 4 index ($r = 0.53$, $p = 0.001$) (table 1). Because the SST variability in the central Pacific is closely related with the Indian Ocean SST through the

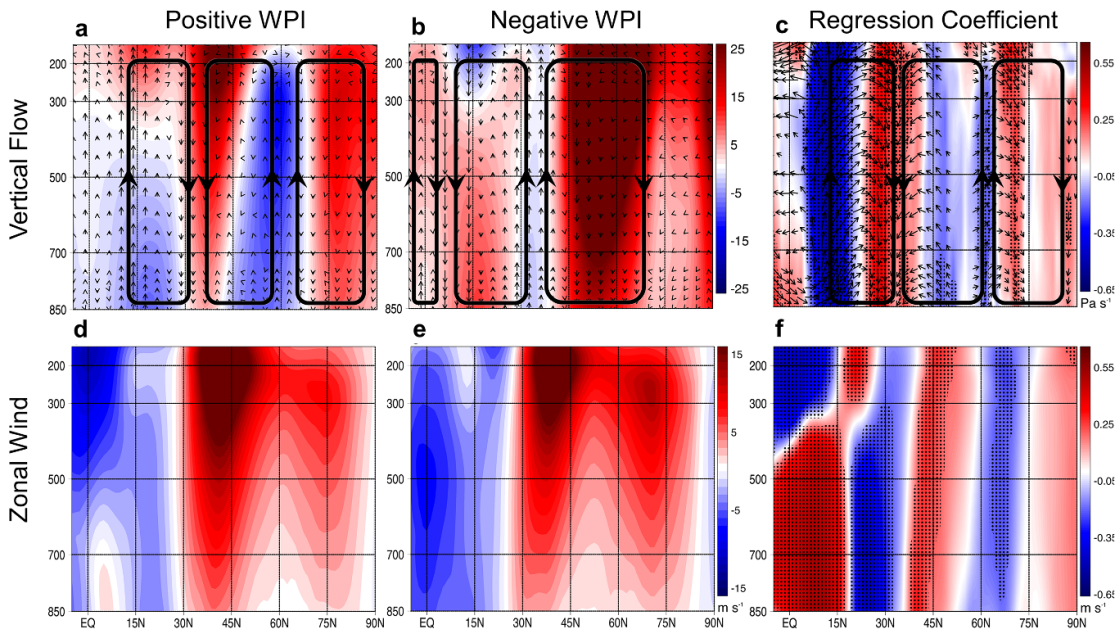

Figure 4. Vertical cross-section of the mean boreal summer meridional circulation averaged over 100 °E–160 °E. The cross-section of mean vertical pressure velocity in a positive (a) and negative (b) phase of WPI, and its regressed coefficient against WPI (c), respectively. In (d)–(f), same with (a)–(c) but for zonal wind. In (a)–(c), the thick black arrows represent the general direction of vertical flow. In (c) a wider and stronger upward (downward) motion in the WPI (midlatitudes) is illustrated. In (d) and (e), the subtropical jet stream near 45 °N intensifies (weakens) and shifts poleward (equatorward) in a positive (negative) WPI phase. In (f) stronger low-level westerlies dominate the tropics and a stronger subtropical jetstream is prominent in the midlatitudes. The black dots indicate significant difference at $p < 0.05$ level, two-tailed distribution.

atmospheric bridge effect of the Pacific Walker Circulation, the partial correlation of the IOBW with the WPI while controlling for the Pacific Walker Circulation index becomes significant ($r = -0.38$, $p = 0.024$) (supplementary table S3). It is reported that the cool IOBW anomalies in JJA prompts anomalous low-level westerlies to flow towards the convective heat source to the east of the Philippines associated with the warm Niño 4 region (TCC 2020b, Basconcillo *et al* 2021). The convergence of the anomalous low-level westerlies with the easterlies in the extended monsoon trough (figure 5(f)) provides background cyclonic vorticity (figure 5(h)), stronger convection (figure 5(b)), and stronger upper-level divergence (figure 5(j)) leading to increased WNP TC genesis. In a negative WPI phase, the opposite effects are illustrated (figures 3(b), 4(b), (e) and 5(b), (d), (f), (h), supplementary figures 2(b) and (e)).

3.2. Possible influence of the WPI on compound climate extremes

The influence of the WPI on compound climate extremes is demonstrated by the significant correlation of WPI with the PRCPTOT, TX90P, and CDD (figures 6(a)–(c)), and TC frequency ($r = 0.60$, $p = 0.000$) (figure 2(a)). The PRCPTOT has significant correlation with WPI in the areas identified in figure 1 such as Vietnam, Myanmar, India, Greece, and Philippines (figure 6(a)). In a positive WPI phase, the said areas experience heavy precipitation events. For example, the northern parts of Greece were affected by heavy precipitation, Kerala, India experienced the worst flood in the recent history (figure 1, supplementary table S1), and the highest TC frequency were recorded in JJA 2018 (Basconcillo *et al* 2021).

Meanwhile, the TX90P and CDD (figures 6(b)–(c)) are also significantly correlated in the areas with extreme warm and dry events in figure 1, particularly in East Asia, Northern Europe, and Eastern United States. The city of Seoul in South Korea set its warmest August in recent history, while several wildfires were recorded in Alaska and Canada in JJA 2018 (figure 1, supplementary table S1), which support that the WPI, as another form of tropical convection index, can possibly influence the occurrence of compound climate extremes.

We emphasize that the negative WPI phase could also result in compound climate extremes. For example, the massive floodings in East Asia, such as the 1998 Yangtze River Flood, which is considered to be among the worst records in China (Ye and Glantz 1998), is captured by a negative WPI phase (figure 6(a)). An example of an extreme temperature event and prolonged dry conditions is shown near the Moscow region, as exemplified by the 2010 Russian heatwave (Francis and Vavrus 2012, Coumou *et al* 2018) (figures 6(b) and (c)). These examples of compound climate extremes imply that both WPI phases can sufficiently detect their occurrence.

Table 1. Correlation of the WPI, WNPMI, and TC frequency with indicated climate index, and the partial correlation of WPI with indicated climate index when controlled for WNPMI.

	WPI (p-value)	WPI control for WNPMI (p-value)	WNPMI (p-value)	TC frequency (p-value)
Meridional circulation system indices (1984–2018)				
East Asian jetstream index	**0.60 (0.000)**	0.24 (0.182)	**0.58 (0.000)**	**0.53 (0.001)**
WNP subtropical high index (WNPSH)	**−0.70 (0.000)**	**0.34 (0.050)**	**−0.91 (0.000)**	**−0.50 (0.003)**
Hadley Cell index	**−0.69 (0.000)**	**−0.43 (0.012)**	**−0.59 (0.001)**	**−0.41 (0.013)**
Ferrel Cell index	**−0.64 (0.000)**	**−0.38 (0.029)**	**−0.56 (0.001)**	**−0.35 (0.039)**
Pacific and Indian Ocean climate indices (1984–2018)				
Niño 4 (N4)	**0.53 (0.001)**	**0.46 (0.006)**	**0.36 (0.034)**	0.30 (0.079)
Indian Ocean basin wide SST (IOBW)	−0.21 (0.218)	0.29 (0.096)	**−0.41 (0.015)**	**−0.49 (0.003)**
Tropical convection and teleconnection indices (1984–2018)				
TC frequency	**0. 60 (0.000)**	0.21 (0.225)	**0.60 (0.000)**	
Pacific Walker circulation index	**−0.40 (0.017)**	−0.18 (0.302)	**−0.37 (0.031)**	−0.14 (0.367)
Circumglobal teleconnection index (CGTI)	0.00 (0.996)	0.00 (0.994)	0.00 (0.999)	0.16 (0.367)
Silk Road pattern (SRP) index	−0.01 (0.953)	−0.11 (0.535)	0.05 (0.759)	0.12 (0.477)
WNP monsoon index (WNPMI)	**0.86 (0.000)**			**0.60 (0.000)**
East Asian summer monsoon index (EASMI)	**−0.82 (0.000)**	**0.37 (0.029)**	**−0.99 (0.000)**	**−0.61 (0.000)**
PJ pattern index (PJ)	**0.41 (0.014)**	−0.12 (0.508)	**0.54 (0.001)**	0.26 (0.127)
Pacific North American pattern (PNA)	−0.18 (0.307)	0.12 (0.490)	−0.28 (0.106)	−0.26 (0.135)
Indian monsoon index	0.10 (0.579)	0.23 (0.196)	−0.02 (0.897)	**0.42 (0.013)**
North Atlantic Ocean climate indices (1984–2018)				
North Atlantic oscillation (NAO)	**0.45 (0.007)**	**0.36 (0.038)**	0.32 (0.063)	**0.57 (0.000)**
Greenland blocking index (GBI)	**−0.39 (0.020)**	**−0.38 (0.027)**	−0.24 (0.174)	**−0.60 (0.000)**
Long-term climate indices (1958–2018)				
Pacific decadal oscillation (PDO)	**0.57 (0.000)**	**0.57 (0.000)**	0.23 (0.093)	
Interdecadal Pacific oscillation (IPO)	**0.40 (0.003)**	**0.50 (0.000)**	0.23 (0.094)	
Atlantic meridional oscillation (AMO)	**0.38 (0.004)**	−0.23 (0.100)	0.14 (0.300)	
North Atlantic oscillation (NAO)	**−0.46 (0.000)**	**0.43 (0.001)**	0.19 (0.141)	
Greenland blocking index (GBI)	**0.48 (0.000)**	**−0.52 (0.000)**	−0.12 (0.357)	

P-values in bold are significant at $p \leqslant 0.05$ confidence level.

3.3. Teleconnection pattern associated with WPI

The WPI is associated with three teleconnection patterns (figure 7(a)). The first pattern is related with the Pacific Walker Circulation ($r = -0.40$, $p = 0.017$) (table 1). Such anticorrelation indicates that the stronger convection center and ascending vertical motion is found in the western Pacific (near 150 °E) and its descent is located in the eastern Pacific (figure 5(b)). The active convective anomalies in the WPI region are likely a Rossby wave response to the central Pacific warm SSTs that increase westerly anomalies drawn from the cold Indian Ocean towards the warm central Pacific (figures 5(f) and (h)). The cyclonic meridional shear vorticity associated with the equatorial westerly anomalies induces the low-level pressure anomalies, eastward extension of the monsoon trough, and enhanced precipitation. The westward extension of the low-pressure from the Philippine Sea to the Bay of Bengal resulting from the westward dispersion of the Rossby waves further enhances the precipitation in the WPI region (Xiang and Wang 2013).

As previously discussed, the WPI is correlated with the meridional circulation indices in the WNP (table 1). Therefore, the second pattern related with the WPI follows a poleward regional meridional circulation that begins with longer waves from the WPI region to the Okhotsk Sea (figures 7(a) and (b)). The direction of the longer waves shows a waveguide pattern in the extratropics splitting and dispersing along the East Asian subtropical jetstream that follows a circumglobal teleconnection—this being the

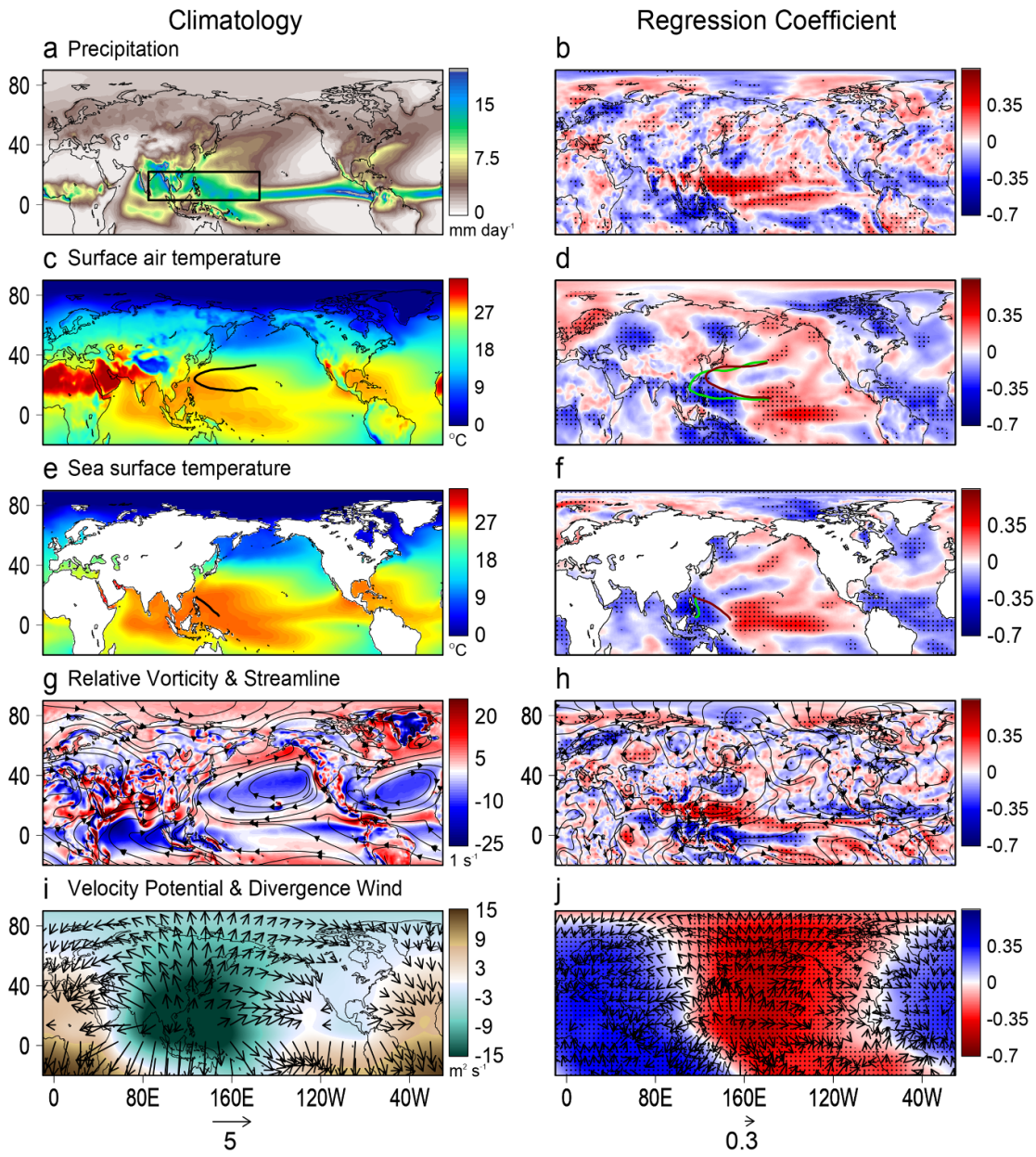

Figure 5. Influence of the WPI on the mean boreal summer. Left panel, mean climatology maps of precipitation (a), surface air temperature (c), SST (e), and 850 hPa relative vorticity and streamline (g). Right panel, regression maps of WPI and corresponding variables. In (a) the black box indicates the location of the WPI region. In (c) and (e) the black line indicates the climatological position of the WNP subtropical high and monsoon trough, respectively. In (d) the red (green) line represents the location of the WNP subtropical high during positive (negative) WPI phase. In (f) same with (d) but shown for the location of the monsoon trough. In (g) the relative vorticity is multiplied with 1000 000 for scaling. The black dots represent significant regression coefficients ($p < 0.05$).

third pattern. Following the Rossby wave tracing theory (Hoskins and Karoly 1981), only longer waves can propagate poleward until they turn at critical latitudes toward the equator. Generally, along the three teleconnection patterns are the locations of compound climate extremes discussed in figures 1 and 6(a)–(c), which imply that the WPI is associated with three teleconnection patterns: the Walker Circulation, the regional meridional circulation in the WNP, and another mode of circumglobal teleconnection pattern.

The WPI-associated circumglobal pattern leads us to a concern on whether the WPI is different from the previously proposed CGTI (Ding and Wang 2005, Ding *et al* 2011). We note that there are striking similarities between the reported teleconnection of CGTI and WPI, which is because both teleconnection patterns are embedded in the waveguide of the subtropical jetstream. However, there is practically no correlation between CGTI and the WPI ($r = 0.00$) (table 1). Additionally, the SRP, which is another teleconnection pattern in the northern Eurasian region that corresponds with the waveguide of the subtropical jetstream, has no correlation with the WPI ($r = -0.01$) (Song *et al* 2013) (table 1).

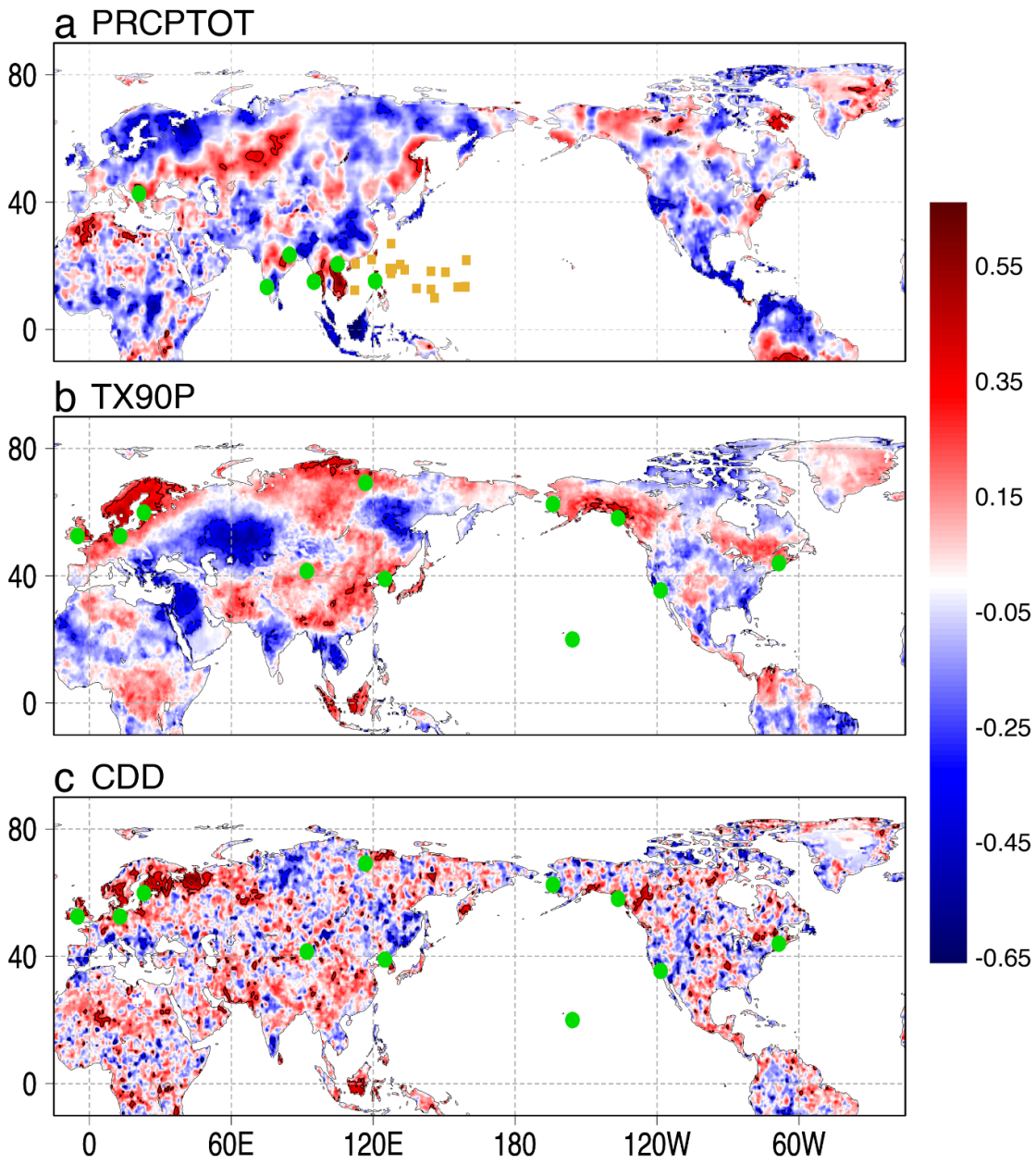

Figure 6. Correlation maps of the WPI with selected climate extreme indices. (a) Amount of total precipitation during wet days (PRPCTOT). (b) Percentage amount of maximum temperature above 90th percentile (TX90P). (c) Number of CDDs. These indices were selected to represent extreme precipitation, extreme temperature, and prolonged dry conditions, respectively. In (a)–(c), the black contour lines represent 95% confidence in the correlation (two-tailed distribution) while the green dots represent the location of extreme events in figure 1. In (a) the orange squares indicate the tropical cyclone genesis locations in JJA 2018.

The difference in the CGTI and WPI is perhaps due to the origin of their respective tropical convective heat sources. The CGTI is proposed to be excited by the Indian summer monsoon (CGTI vs Indian monsoon index, $r = 0.35$, $p = 0.040$) while the WPI is a combination of the in-phase intense convective centers in the WNP and the Bay of Bengal (Wang *et al* 2001) (figure 5(a)). It is previously emphasized that the two Asian summer monsoons (e.g. Indian and WNP summer monsoon) are not necessarily independent from each other but they may have combining relationship in certain years (Wang *et al* 2001). For example, the two summer monsoons were in-phase in 1994, which is regarded as the one of the major flood years in India since 1988 (IITM 2017). In the same year, the WPI was active. Therefore, it stands to reason that the WPI could also initiate a waveguide pattern that is different from that of the Indian summer monsoon. At this point, we underscore that the negative correlation patterns of the CGTI with 700 hPa geopotential height is significant only in the northwestern Indian Ocean denoting that two circumglobal teleconnection patterns (vis-à-vis WPI) have different convective heat sources (figure 8(e)). This also indicates that the CGTI cannot describe the intense convection center in the WNP, which accounts for the

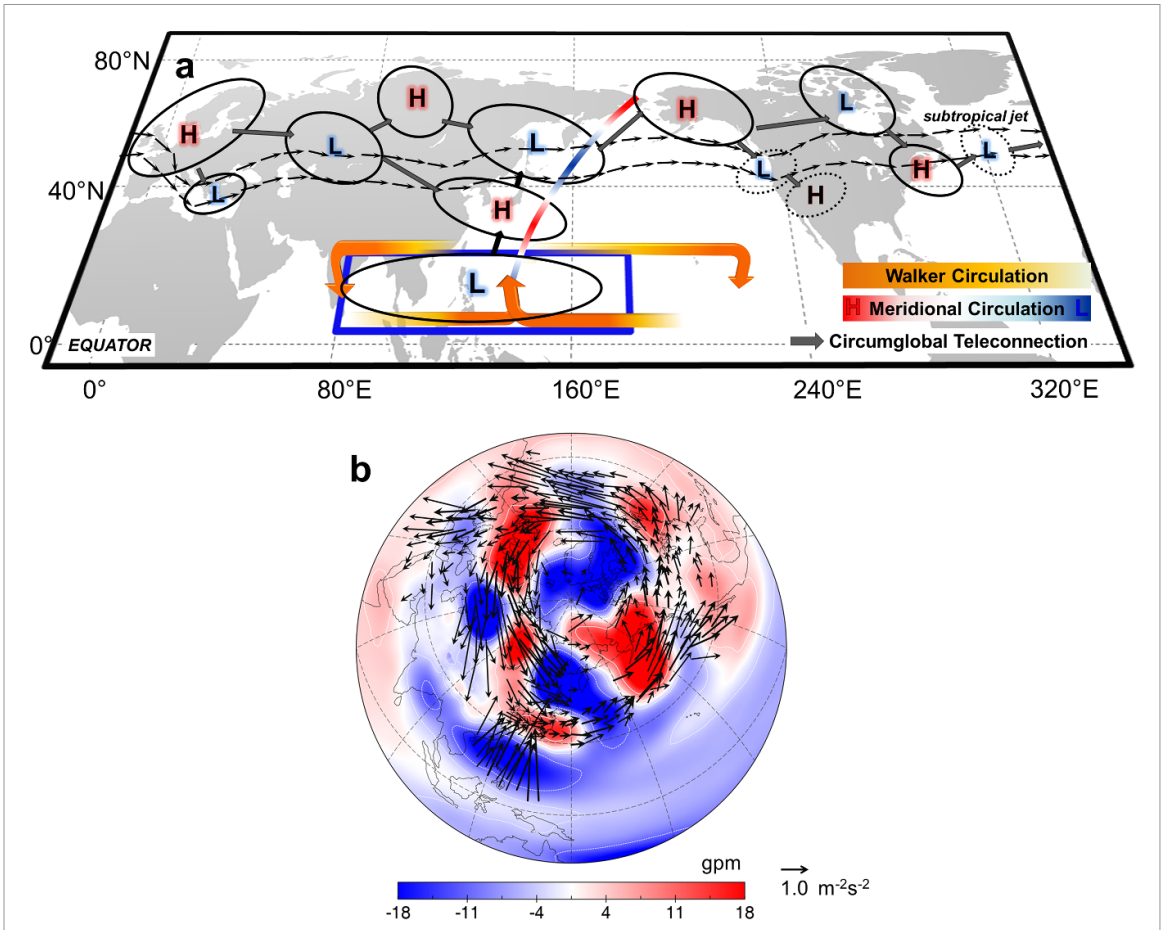

Figure 7. Teleconnection patterns associated with the WPI. (a) Schematic of the three teleconnection patterns associated with the WPI. The moist air converges and rises in the WPI region (i.e. Walker circulation) prompting an anomalous convective activity that generates a poleward train of pressure anomalies (i.e. meridional circulation). A waveguide pattern in the extratropics along the waveguide of the subtropical jetstream follows a circumglobal teleconnection—this being the third pattern. The thick (thin) arrows indicate the direction of the circumglobal pattern (subtropical jetstream). The L (H) denotes a low (high) pressure region. The blue box represents the WPI region. (b) The composite difference map in 700 hPa mean geopotential height between positive and negative WPI phases. In a positive WPI phase, the arrows indicate the direction of 700 hPa wave activity flux beginning from the WPI region.

active TC genesis and heavy precipitation in the WNP. Therefore, the WPI presents an added value that it is different from the CGTI-associated patterns.

3.4. Comparison of the WPI with known tropical convection indices

A number of tropical convection indices such as the WNPMI (Wang *et al* 2001) and the PJ pattern (Wakabayashi and Kawamura 2004) are previously reported to be associated with a meridional teleconnection pattern. The WPI is significantly correlated with the WNPMI ($r = 0.86$, $p = 0.000$), EASMI ($r = -0.82$, $p = 0.000$), and PJ pattern ($r = 0.41$, $p = 0.014$) (table 1), respectively. In general, the EASMI is the reverse form of the WNPMI ($r = -0.99$, $p = 0.000$). We proceed to use the WNPMI and PJ in our succeeding analysis because they directly correlated with the WPI. Meanwhile, the PNA pattern, which is considered to be the downstream impact of the ENSO in the eastern equatorial Pacific (Harding and Snyder 2015), has no significant correlation with the WPI, WNPMI, and TC frequency. Such insignificant correlation is, perhaps because the PNA pattern is more pronounced in the eastern equatorial Pacific during the boreal winter (Harding and Snyder 2015, Oh *et al* 2018).

It is, therefore, another concern whether the WPI merits consideration of its potential application that is different from the WNPMI and PJ. It should be noted that the WNPMI and PJ pattern were primarily developed to explain manifestation and mechanism of regional climate systems (e.g. monsoon, PJ climate dynamics). To reiterate, we do not attempt to discount the merits of the said indices, but rather we aim to build on their known mechanism in explaining the global teleconnection of compound climate extremes.

We show that the partial correlation patterns of WPI against the 700 hPa geopotential height when the influence of WNPMI and PJ are respectively controlled remain significant over the Greenland region, Baffin Bay, some parts of East Asia, Okhotsk Sea, eastern United States, central Russia, northern Europe, and the Mediterranean (figures 8(a)–(d)).

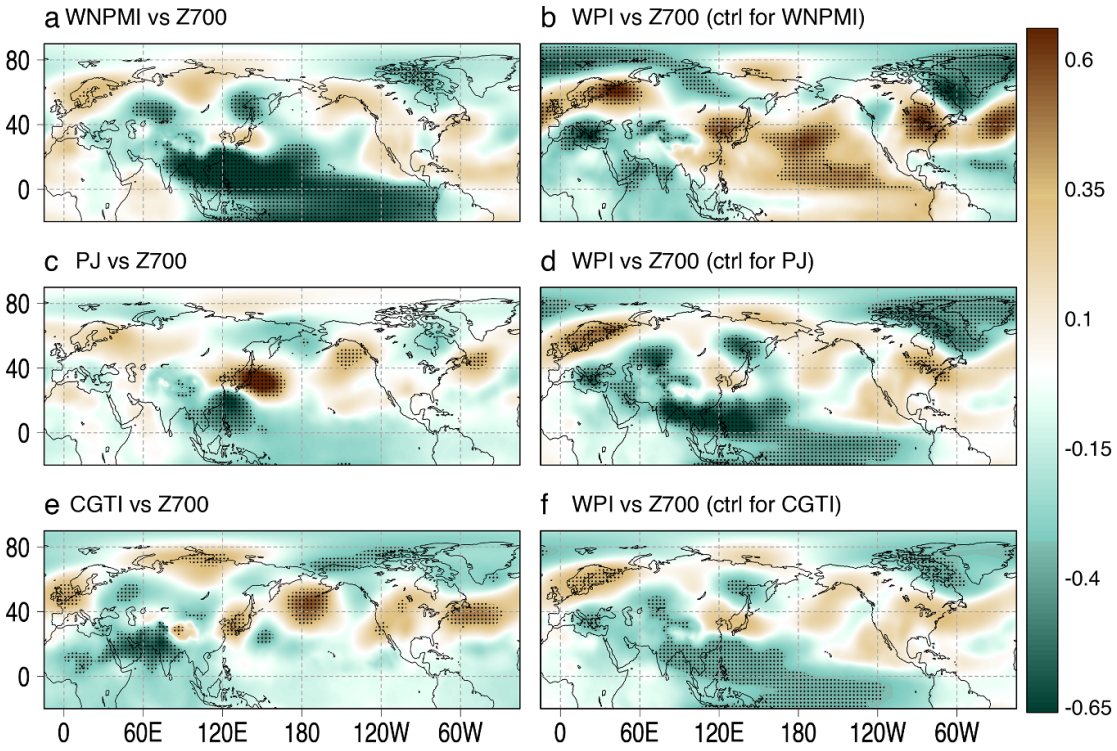

Figure 8. Partial correlation maps of indicated climate index and 700 hPa mean geopotential height from 1984 to 2018. Left panel, correlation maps between 700 hPa mean geopotential height and indicated climate index. Right panel, partial correlation maps of the WPI and 700 hPa mean geopotential height when the influence of indicated climate index is controlled. The black dots represent 95% confidence in the correlation (two-tailed distribution).

Meanwhile, there is no significant correlation found in the original correlation map of WNPMI and PJ (and CGTI) against 700 hPa geopotential height in the said areas—most notably in the Greenland region. We also confirm that there is no significant correlation between WNPMI and PJ, and the North Atlantic Ocean climate indices, respectively (table 1), which support that the said tropical convection indices could not completely capture the waveguide pattern associated with the WPI. Furthermore, when the WPI is controlled for WNPMI and PJ (and CGTI), the WPI remains correlated with the NAO and GBI (table 1, supplementary table S3).

A positive NAO and a negative GBI is associated with colder climate near the Greenland region and in the Mediterranean, but warmer climate in most parts of northern Europe. A reverse climate pattern is observed in a negative NAO (Folland *et al* 2009) and positive GBI (Hanna *et al* 2013). Moreover, the NAO and GBI can explain the undulation of the North Atlantic subtropical jetstream. With this, we show that the WPI has significant partial correlation with the 300 hPa zonal wind in northern Scandinavia (figures 9(b), (d), (f)), which is not found in the partial correlation of WNPMI, and PJ, respectively. A positive correlation means stronger subtropical jetstream and northward shift in the North Atlantic subtropical jetstream, which allows warm tropical air mass to stall in United Kingdom and many parts of Europe.

At this point, we have demonstrated that the small differences in the recipes of tropical convection indices account for the significant differences in their respective teleconnection patterns. Therefore, the WPI presents new contribution by describing teleconnection patterns that may not be necessarily independent, but significantly different from the previously reported teleconnection patterns of known tropical convection indices.

The last concern that needs to be addressed is whether such correlation persists even in longer period. The significant correlations of WPI with the NAO ($r = 0.46$, $p = 0.000$) and GBI ($r = -0.48$, $p = 0.00$) from 1958 to 2018 (JRA-55 reanalysis period begins in 1958) remain significant, respectively (table 1). Moreover, the significant partial correlations of WPI with NAO ($r = 0.43$, $p = 0.001$) and GBI ($r = -0.52$, $p = 0.000$) when controlled for the WNPMI also remain significant, respectively (table 1). These findings suggest the persistence of WPI-associated teleconnection patterns even in longer period (i.e. 1958–2018), which, warrant WPI its merits in providing new insights on the teleconnection of compound climate extremes.

3.5. Trend and variability of the WPI

There is no trend in WPI from 1984 to 2018 but there is a significantly increasing trend in WPI values if the analysis period is extended back to 1958 (supplementary figure S3(a)). Among the long-term

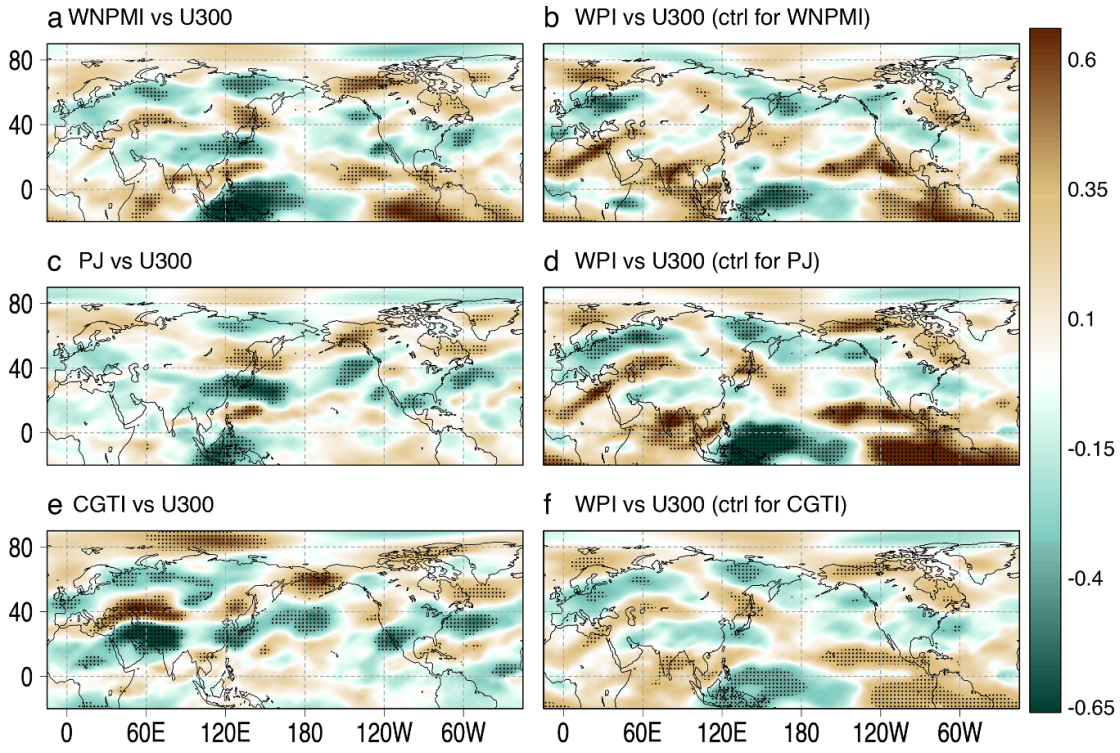

Figure 9. Partial correlation maps of indicated climate index and 300 hPa mean zonal wind from 1984 to 2018. Left panel, correlation maps between 300 hPa mean zonal wind speed and indicated climate index. Right panel, partial correlation maps of the WPI and 300 hPa mean zonal wind speed when the influence of indicated climate index is controlled. The black dots represent 95% confidence in the correlation (two-tailed distribution).

climate indices, the PDO ($r = 0.57$, $p = 0.000$) (table 1) has the highest correlation with the WPI so we reduced the PDO influence from the WPI by detrending the WPI timeseries with respect to PDO. The significant trend persists after such reduction, which suggests increasing tropical convective activity in the WPI region. Moreover, we found that the WNPMI has marginal but increasing trend (supplementary figure S4(a)) while the PJ pattern has significant decreasing trend (supplementary figure S4(b)). The consistent trends of the WPI, WNPMI, and PJ pattern, respectively, support the increasing signal in tropical convective activities in the WNP. Meanwhile, there is no significant trend in CGTI (supplementary figure S4(c)).

Using the Paul wavelet transform, we show that the WPI from 1984 to 2018 has high-frequency variability every 3–4 years and low-frequency variability every 10–12 years (supplementary figure S3(b)). Such periodicities have important implications in the predictability of WPI and compound climate extremes. For instance, the Yangtze River floodings, which is an event that is possibly tied to a negative WPI phase, is reported to occur almost every 10 years in the last 2000 years (Ye and Glantz 1998).

3.6. Possible relationship of TCs to the other climate extremes

The relationship of TCs with the other climate extremes beyond the tropics is not well understood. Our study contributes in filling this knowledge gap by showing that the TCs in the WNP, as another form of active tropical convection, can influence the meridional circulation in the WNP during JJA. This is supported by the significant correlation of TC frequency with the East Asian Subtropical Jetstream index ($r = 0.53$, $p = 0.001$), WNP Subtropical High index ($r = -0.50$, $p = 0.003$), Hadley Cell index ($r = -0.41$, $p = 0.013$), and Ferrel Cell index ($r = -0.35$, $p = 0.039$) (table 1). Furthermore, the TC frequency is also well correlated with NAO ($r = 0.57$, $p = 0.000$) and GBI ($r = -0.60$, $p = 0.000$). Thus, it can be argued that the TCs in the WNP during JJA can possibly excite the teleconnection of compound climate extremes, more particularly in the North Atlantic region, in the same way as the associated teleconnection patterns of the WPI.

4. Discussion and conclusion

Here we presented robust observational evidence on how the interannual variations in the Indo-Pacific warm pool convection, which we call as the WPI, could possibly influence three major teleconnection patterns in the meridional, zonal, and circumglobal directions (figure 7(a)). Generally, along these teleconnection patterns are the regions of compound climate extremes (figures 6(a)–(c)). Although the magnitude of WPI influence on compound

climate extremes may vary across positive/negative WPI years, the large-scale climate anomalies associated with the WPI are likely to remain consistent, even in longer periods. Note that the correlations of the WPI with NAO and GBI, respectively, remain significant even in longer period (i.e. 1958–2018). Therefore, understanding the variability of the WPI, including its predictability, could pave way for the seasonal prediction of compound climate extremes, particularly during the boreal summer.

Although our analysis only covers until 2018, we note that the WPI was in its negative phase during the JJA 2020 (WPI $= -1.5$), which means that the compound climate extremes recorded in the said year are possibly influenced by the WPI. These extreme events include the below normal TC frequency in WNP, and massive floodings in South and East Asia (World Meteorological Organization (WMO) 2020a), extreme temperatures in the Canadian Archipelago (World Meteorological Organization (WMO) 2020b), and prolonged heat in central Russia (World Meteorological Organization (WMO) 2020c), which are captured by the WPI in its negative phase (figures 6(a)–(c)).

In addition, the tug-of-war [5] for the subtropical jetstream that is happening between the Arctic and tropics is, in fact, a case of caught in the middle, particularly for the midlatitudes. While it is not yet fully understood which of these competing forces will dominate the subtropical jetstream, compound climate extremes in many parts of the extratropics could be exacerbated with global warming.

We fully recognize that our findings in its current form are dependent on observational analysis but we also have presented robust evidence that warrant WPI its merits. In this regard, we plan to extend our future work on the numerical investigation of the WPI and its sensitivity to the other large-scale climate systems. We do not explicitly subscribe our findings with anthropogenic climate change because of the temporal limitations of our analysis. While we have shown that the WPI have significantly increased since 1958, whether such increasing trend is a footprint of anthropogenic climate change and/or other multiyear external climate variability is yet to be determined. What is more pressing, however, is to investigate the implication of such trends to compound climate extremes, at least within the historically recorded realm. Finally, with the simplicity of our proposed WPI index, we have demonstrated the potential application of WPI to detect compound climate extremes and to provide better insights on disaster risk reduction.

Data materials availability

The reanalysis products used in this study are available for download from their respective websites.

Data availability statement

All data that support the findings of this study are included within the article (and any supplementary files).

Acknowledgments

The authors would like to express their gratitude to the following individuals in helping them prepare the manuscript: Mr Chris John Delantes, Ms Julie Ann Basconcillo, Mr Raymond Ordinario, Ms Rhonalyn Macalalad, and Dr Reniel Pamplona. Likewise, authors would like to acknowledge the following institutions for the data products used in this study: the Interactive Assessment of the Climate Systems–Tokyo Climate Center and Physical Sciences Laboratory-National Oceanic and Atmospheric Administration.

Funding

This work was supported by the Basic Science Research Program, through the National Research Foundation of Korea (NRF) funded by the Ministry of Education (2017R1A2B2005019) and a part of the project titled 'Improvements of ocean prediction accuracy using numerical modeling and artificial intelligence technology', funded by the Ministry of Oceans and Fisheries, Korea. M N M was supported by a grant funded by the European Research Council (ERC) under the European Union's Horizon 2020 research and innovation programme with Grant Agreement No. 756194 (ENERGYA).

Author contributions

J Q B and I J M designed and conducted the study. M N M provided the gridded climate extreme indices. J Q B, I J M, M N M, and B W wrote and reviewed the manuscript.

Conflict of interest

None declared.

ORCID iDs

Il-Ju Moon https://orcid.org/0000-0001-9370-0900
Malcolm Mistry https://orcid.org/0000-0003-3345-6197

References

Adler R *et al* 2003 The version-2 global precipitation climatology project (GPCP) monthly precipitation analysis (1979–Present) *J. Hydrometeorol.* **4** 1147–67

Basconcillo J, Cha E J and Moon I J 2021 Characterizing the highest tropical cyclone frequency in the Western North Pacific since 1984 *Sci. Rep.* **11** 14350
Bintanja R and van der Linden E 2013 The changing seasonal climate in the Arctic *Sci. Rep.* **3** 1556
Chen S, Ke W, Wen C and Linye S 2014 Regional changes in the annual mean Hadley circulation in recent decades *J. Geophys. Res. Atmos.* **119** 7815–32
Cohen J *et al* 2014 Recent Arctic amplification and extreme mid-latitude weather *Nat. Geosci.* **7** 627–37
Coumou D, Di Capua G, Wang L and Wang S 2018 The influence of Arctic amplification on mid-latitude summer circulation *Nat. Comm.* **9** 2959
Ding Q and Wang B 2005 Circumglobal teleconnection in the Northern Hemisphere summer *J. Clim.* **18** 3484–505
Ding Q, Wang B, Wallace J and Branstator G 2011 Tropical–extratropical teleconnections in boreal summer: observed interannual variability *J. Clim.* **24** 1878–96
Emanuel K 2005 Increasing destructiveness of tropical cyclones over the past 30 years *Nature* **436** 686–8
Evans J 1993 Global guide to tropical cyclone forecasting *World Meteorological Organization*
Folland C, Knight J, Linderholm H, Fereday D, Ineson S and Hurrel J 2009 The summer North Atlantic oscillation: past, present, and future *J. Clim.* **22** 1082–103
Francis J and Vavrus S 2012 Evidence linking Arctic amplification to extreme weather in mid-latitudes *Geophys. Res. Lett.* **39** L06801
Gadgil S 2018 The monsoon system: land–sea breeze or the ITCZ? *J. Earth Sys. Sci.* **127** 1
Hanna E, Jones J, Cappelen J, Mernild S, Wood L, Steffen K and Huybrechts P 2013 The influence of North Atlantic atmospheric and oceanic forcing effects on 1900–2010 Greenland summer climate and ice melt/runoff *Int. J. Clim.* **33** 862–88
Harding K and Snyder P 2015 The relationship between the Pacific–North American teleconnection pattern, the Great Plains low-level jet, and north central US heavy rainfall events *J. Clim.* **28** 6729–42
Hoskins B and Karoly D 1981 The steady linear response of a spherical atmosphere to thermal and orographic forcing *J. Atmos. Sci.* **38** 1179–96
Huang D, Zhu J, Zhang Y and Huang A 2014 The different configurations of the East Asian polar front jet and subtropical jet and the associated rainfall anomalies over eastern China in summer *J. Clim.* **27** 8205–20
Indian Institute of Tropical Meteorology (IITM) 2017 Interannual variations of Indian summer monsoon *Indian Monsoon Rainfall Record of the Past Century*
Intergovernmental Panel on Climate Change (IPCC); The Physical Science Basis 2021 Summary for policymakers *Climate Change* (Cambridge: Cambridge University Press) pp 1–41
Kalnay E *et al* 1996 The NCEP/NCAR 40-year reanalysis project *Bull. Am. Meteorol. Soc.* **77** 437–71
Kang N and Elsner J 2012 Consensus on climate trends in western North Pacific tropical cyclones *J. Clim.* **25** 7564–73
Kendall M 1975 *Rank correlation methods* 4th edn (London: Charles Griffin) p 202
Kim M H and Moon I J 2021 Evaluation of the reliability of tropical cyclone data using ENSO *Asia Pacific J. Atmos. Sci.* (https://doi.org/10.1007/s13143-021-00260-3)
Knapp K R, Kruk M C, Levinson D H, Diamond H J and Neumann C J 2010 The International Best Track Archive for Climate Stewardship (IBTrACS) *Bull. Amer. Meteor. Soc.* **91** 363–76
Kobayashi S *et al* 2015 The JRA-55 reanalysis: general specifications and basic characteristics *J. Meteorol. Soc. Japan* **93** 5–48
Li X, Li J, Zhang X and Sun C 2014 Role of Ferrel cell in daily variability of Northern Hemisphere annular mode *Chin. Sci. Bull.* **59** 3457–64
Mann H 1945 Non-parametric tests against trend *Econometrica* **13** 163–71
Mistry M 2019 A high-resolution global gridded historical dataset of climate extreme indices *Data* **4** 41
National Oceanic and Atmospheric Administration (NOAA) 2020 *Climate Indices: Monthly Atmospheric and Ocean Time-Series* (available at: https://psl.noaa.gov/data/climateindices/list/) (Accessed 21 November 2020)
Nitta T 1987 Convective activities in the tropical western Pacific and their impact on the Northern Hemisphere summer circulation *J. Meteorol. Soc. Japan* **65** 373–90
Oh H R, Ho C H, Par D S, Kim J W, Song C K and Hur S K 2018 Possible relationship of weakened Aleutian low with air quality improvement in Seoul, South Korea *J. Appl. Meteorol. Clim.* **57** 2363–73
Rienecker M *et al* 2011 MERRA: NASA's modern-era retrospective analysis for research and applications *J. Clim.* **24** 3624–48
Schneider T, Bischoff T and Haug G 2014 Migrations and dynamics of the intertropical convergence zone *Nature* **513** 45–53
Schneider T, O'gorman P and Levine X 2010 Water vapor and the dynamics of climate changes *Rev. Geophys.* **48** 1–22
Song F, Leung R, Lu J and Dong L 2018a Future changes in seasonality of the North Pacific and North Atlantic subtropical highs *Geophys. Res. Lett.* **45** 11959–68
Song F, Leung R, Lu J and Dong L 2018b Seasonally-dependent responses of subtropical highs and tropical rainfall to anthropogenic warming *Nat. Clim. Change* **8** 787–92
Song F and Zhou T 2014a The climatology and inter-annual variability of East Asian summer monsoon in CMIP5 coupled models: does air-sea coupling improve the simulations? *J. Clim.* **27** 8761–77
Song F and Zhou T 2014b Inter-annual variability of East Asian summer monsoon simulated by CMIP3 and CMIP5 AGCMs: skill dependence on Indian Ocean-western Pacific anticyclone teleconnection *J. Clim.* **27** 1679–97
Song F, Zhou T and Wang L 2013 Two modes of the Silk Road pattern and their inter-annual variability simulated by LASG/IAP SAMIL2.0 *Adv. Atmos. Sci.* **30** 908–21
Staten P, Lu J, Grise K, Davis S and Birner T 2018 Re-examining tropical expansion *Nat. Clim. Change* **8** 768–75
Takaya K and Nakamura H 2001 A formulation of a phase-independent wave-activity flux for stationary and migratory quasigeostrophic eddies on a zonally varying basic flow *J. Atmos. Sci.* **58** 608–27
Tokyo Climate Center (TCC) 2020a *El Niño Monitoring Indices* (available at: https://ds.data.jma.go.jp/tcc/tcc/products/elnino/index/index.html) (Accessed 21 November 2020)
Tokyo Climate Center (TCC) 2020b *Composite map for El Niño/La Niña and Indian Ocean Dipole events* (available at: https://ds.data.jma.go.jp/tcc/tcc/products/clisys/enso_statistics/index.html) (Accessed 21 November 2020)
Torrence C and Compo G 1998 A practical guide to wavelet analysis *Bull. Am. Meteorol. Soc.* **79** 1
Trouet V, Babst F and Meko M 2018 Recent enhanced high-summer North Atlantic Jet variability emerges from three-century context *Nat. Comm.* **9** 180
Vecchi G, Soden B, Wittenberg A, Held I, Leetmaa A and Harrison M 2006 Weakening of tropical Pacific atmospheric circulation due to anthropogenic forcing *Nature* **441** 73–76
Wakabayashi S and Kawamura R 2004 Extraction of major teleconnection patterns possibly associated with the anomalous summer climate in Japan *J. Meteorol. Soc. Japan* **82** 1577–88
Wang B and Fan Z 1999 Choice of South Asian summer monsoon indices *Bull. Am. Meteorol. Soc.* **80** 629–38
Wang B, Wu R and Lau K 2001 Interannual variability of the Asian summer monsoon: contrasts between the Indian and the western North Pacific–East Asian monsoons *J. Clim.* **14** 4073–90
Wang B, Wu Z, Li J, Liu J, Chang C, Ding Y and Wu G 2008 How to measure the strength of the East Asian summer monsoon? *J. Clim.* **21** 4449–63
Wang B, Xiang B and Lee J 2013 Subtropical high predictability establishes a promising way for monsoon and

tropical storm predictions *Proc. Natl Acad. Sci.* **110** 2718–22

Wang C, Wang B and Cao J 2019 Unprecedented northern hemisphere tropical cyclone genesis in 2018 shaped by subtropical warming in the North Pacific and the North Atlantic *Geophys. Res. Lett.* **46** 13327–37

Watt-Meyer O and Frierson D 2018 ITCZ width controls on Hadley cell extent and eddy-driven jet position and their response to warming *J. Clim.* **32** 1151–66

World Meteorological Organization (WMO) 2020a *Heavy rains and flooding hit large parts of Asia* (available at: https://public.wmo.int/en/media/news/heavy-rains-and-flooding-hit-large-parts-of-asia) (Accessed 21 November 2020)

World Meteorological Organization (WMO) 2020b *Northern Hemisphere Summer 2020 - Extreme events in the ice shelves and glaciers of the world* (available at: https://public.wmo.int/en/our-mandate/focus-areas/cryosphere/Northern-Hemisphere-Summer-2020) (Accessed 21 November 2020)

World Meteorological Organization (WMO) 2020c *Prolonged Siberian heat "almost impossible without climate change"* (available at: https://public.wmo.int/en/media/news/prolonged-siberian-heat-almost-impossible-without-climate-change) (Accessed 21 November 2020)

Xiang B and Wang B 2013 Mechanisms for the advanced Asian summer monsoon onset since the mid-to-late 1990s *J. Clim.* **26** 1993–2009

Ye Q and Glantz M 1998 The 1998 Yangtze floods: the use of short-term forecasts in the context of seasonal to interannual water resource management *Mitigation Adapt. Strategies Global Change* **10** 159–82